Fault-tolerant control of fixed wing UAVs with multiple control surfaces

Wang [illegible]	Ju Jia*	Zhuang [illegible]	Tian [illegible]
Nanchang Hangkong University	Nanchang Hangkong University	Nanchang Hangkong University	Nanchang Hangkong University
Nanchang, China	Nanchang, China	Nanchang, China	Nanchang, China
[illegible]	[illegible]	[illegible]	[illegible]

***Abstract*—An adaptive filtered backstepping method is proposed to solve the expected torque problem caused by various internal unmodeled dynamics, system uncertain parameters, and unknown input gains generated when the control surface of a multi-control surface UAV malfunctions. The fault-tolerant control method utilizes quadratic programming to redistribute control to the remaining control surfaces based on rudder effectiveness. In order to improve control accuracy, an RBF neural network is used to identify and compensate for unmatched disturbances to solve the problem of high complexity of fault-tolerant control technology for existing UAV actuators. Fault-tolerant control of UAV attitude is realized to enhance the survival rate when the control surface fails during UAV flight.**

Keywords—Control surface failure; adaptive filtering backstepping method; quadratic programming; RBF neural network

I. Introduction

Control surface are necessary components for UAVs to change their flight attitude. With the development of large-scale UAVs, in order to improve the reliability and maneuverability of UAVs, there are generally multiple sets of control surfaces on UAVs, forming backup and redundancy with each other. For the sake of fully utilize the control redundancy between control surfaces, it is indispensable to use control allocation techniques [1-3]. The pseudo inverse method takes the quadratic norm of the control variables as the optimization index, and the adjustment of the weighting matrix can weight each control variable and allocate actuator parameters according to the weight values [4,5]. The linear programming method can transform the control allocation problem into a standard linear programming problem based on the optimization objective, which is minimizing the attitude angle error and the control surface deviation angle [6,7]. However, this method is prone to saturation and chattering caused by the simple allocation of control surfaces with limited conditions, and excessive deviation of the control surface which can easily cause the attitude of the UAV to diverge. The quadratic programming method can flexibly utilize the cost functions and current steering effects to enable UAVs to solve complex control allocation problems according to specific constraints[8]. The unmanned aerial vehicle is treated as a linear parametric system, and combined with robust predictive control, so that the quadratic programming algorithm can be used for control allocation, effectively suppressing the impact of changes in control surface efficiency [9]. In order to prevent the control surface from shaking and saturation, this article sets anti-sinking and anti-saturation terms in the cost function when allocating the control torque, so that the control surface deviation angle solved by the quadratic programming not only meets the control requirements but also is small and smooth.

The above method transforms the control allocation problem into a static optimization problem without considering the dynamics of the actuator and the stability of the closed-loop system after using control allocation. The cruising speed of the UAV controlled in this article is high, and the dynamics of the control surface actuator cannot be ignored. Therefore, the second-order link of the servo is added to the simulation. In order to improve the accuracy of UAV control, the aerodynamic data adopt a table lookup interpolation, which avoids the problem of high-order nonlinear terms in the steering effect using fitting at different control surface angles of deviation, attack, and sideslip[10]. The control law adopts a backstepping nonlinear controller derived from the dynamic model. However, traditional sliding mode control algorithms have discontinuous switching logic that can lead to jitter [11-13]. To prevent the differential explosion of the virtual control quantity in the backstepping method, the virtual control quantity is suppressed by multiplying it by a coefficient [14]. When the system contains unknown bounded parameters, the modeling error can be reflected through unknown adaptive terms [15]. In order to enhance the system's anti-interference ability and prevent differential explosion, the filtering adaptive backstepping method is used to solve the desired torque required for control in this article.

Since the adaptive term is a set of unmatched and disturbance terms [16-18], when the system parameters change, adaptive term is approximated through RBF neural networks. The adaptive control term is used to enhance the closed-loop stability of the system and improve transient performance.

This paper takes the floating and missing of control surfaces as an example, and uses the adaptive filtering backstepping method to solve the expected torque. The quadratic programming redistributes the control on the remaining control surfaces based on the rudder effect, and the RBF neural network identifies and compensates for unmatched interference terms. As the aerodynamic performance of UAVs can be affected by many factors, this paper utilizes time-varying nonlinear aerodynamic parameters to improve control accuracy. The control law designed in this article has been validated through simulation, and the attitude tracking error quickly converges to zero when the control surface is jammed. Unlike current typical control surface failures, it can still ensure the controllability of the UAV, thereby improving UAVs' survival rate.

II. DYNAMIC MODEL OF UAV

The UAV attitude angular velocity equation can be written as follows:

$$\dot{\omega}=-J^{-1}S(\omega)J\omega+J^{-1}M \tag{1}$$

$\omega=[p \quad q \quad r]^T$ is attitude angular velocity matrix, J is the moment of inertia matrix of UAV. $S(\omega)$ is the antisymmetric matrix of ω. M is total torque of UAV. The reverse torsion moment and gyro moment generated by the turbojet engine are ignored, so the moment can be regarded as the moment generated by the aerodynamics in the body coordinate system of the UAV. The inertia product J_{xz} of the UAV is very small, approximately 0. In the equation
$J=\begin{bmatrix} J_{xx} & 0 & 0 \\ 0 & J_{yy} & 0 \\ 0 & 0 & J_{zz} \end{bmatrix}$, $S(\omega)=\begin{bmatrix} 0 & -r & q \\ r & 0 & -p \\ -q & p & 0 \end{bmatrix}$.

UAV aerodynamic torque $M=[l_A \quad m_A \quad n_A]^T$ can be written in the following form, $\Phi_1=[1 \quad \alpha \quad \beta \quad p \quad q \quad r]^T$.

$$M=\Theta_1\Phi_1+\Theta_2 u_\delta \tag{2}$$

$\Theta_1=QS\begin{bmatrix} b & 0 & 0 \\ 0 & \bar{c} & 0 \\ 0 & 0 & b \end{bmatrix}\begin{bmatrix} C_{l0} & 0 & C_l^\beta & C_l^p & 0 & C_l^r \\ C_{m0} & C_m^\alpha & 0 & 0 & C_m^q & 0 \\ C_{n0} & 0 & C_n^\beta & C_n^p & 0 & C_n^r \end{bmatrix}$ is stable torque brought in the wings and fuselage. $\Theta_2=QS\begin{bmatrix} b & 0 & 0 \\ 0 & \bar{c} & 0 \\ 0 & 0 & b \end{bmatrix}\begin{bmatrix} C_l^{\delta al} & C_l^{\delta ar} & C_l^{\delta fl} & C_l^{\delta fr} & C_l^{\delta el} & C_l^{\delta er} & C_l^{\delta r} \\ C_m^{\delta al} & C_m^{\delta ar} & C_m^{\delta fl} & C_m^{\delta fr} & C_m^{\delta el} & C_m^{\delta er} & C_m^{\delta r} \\ C_n^{\delta al} & C_n^{\delta ar} & C_n^{\delta fl} & C_n^{\delta fr} & C_n^{\delta el} & C_n^{\delta er} & C_n^{\delta r} \end{bmatrix}$ is control efficiency matrix for various control surfaces of UAV, Q is dynamic pressure, u_δ is control amount for each control surface of the drone.

Figure 1 UAV and its Control Surface

The UAV is shown in Figure 1, with a pair of ailerons and flaps on the main wing, a pair of elevators on the V-tail, and a fully moving vertical tail below the belly.

The UAV control surface faults analyzed in this article are the following:

(1) The control surface floats, meaning that the random wing of the control surface oscillates freely around the flow and cannot continue to respond to control commands. This type of fault can cause the control surface to lose its ability to generate torque on the body.

(2) The control surface is defecting, which means that the control surface can continue to respond to control commands, but due to the reduction of the control surface area, the control gain decreases and the expected control effect cannot be achieved.

Model the control surface with input as $\delta(t)$. The deflection angle range of ailerons, elevators, and rudder is $[-30°, 30°]$, the deflection angle range of flaps is $[0°, 30°]$. The upward deviation of the control surface is negative, the downward deviation is positive, and the right deviation of the full action rudder is negative, and the left deviation is positive. $k_i(t)\in[0,1]$, the expression is as follows:

$$u_\delta(t)=\begin{cases} \delta(t), t\geq 0, & \text{No fault} \\ k_i(t)\delta(t), t\geq t_p, & \text{Control surface defect} \\ 0, t\geq t_j, & \text{Control surface floating} \end{cases} \tag{3}$$

In the simulation, the transfer function of the servo controlling each control surface is simplified as second-order, with a damping ratio of 0.7 and a natural frequency of 62.8.

III. CONTROL LAW DESIGN

A. Adaptive filtering backstepping method for calculating expected torque

The goal of the UAV attitude system tracking controller is to enable the attitude angle tracking error to converge to zero in a finite time. Design adaptive control terms to compensate for disturbances and approximate process errors in the presence of unmodeled dynamics and external disturbances, in order to enhance system closed-loop stability and improve transient performance.

Taking the design of roll angle control law as an example. The state space expression of the rolling total system is:

$$\begin{cases} \dot{\phi}=p \\ \dot{p}=\dfrac{J_{yy}-J_{zz}}{J_{xx}}qr+\dfrac{1}{J_{xx}}l_\delta+\dfrac{1}{J_{xx}}M_{ex} \end{cases} \tag{4}$$

Set $f(\omega)$ and $g(\omega)$ in the following form, M_{ex} is interference torque on the x-axis of the body coordinate.

$$f(\omega)=\frac{J_{yy}-J_{zz}}{J_{xx}}qr+\frac{1}{J_{xx}}M_{ex}$$
$$g(\omega)=\frac{1}{J_{xx}} \tag{5}$$

$$e_{r1} = \phi_d - \phi \tag{6}$$

Taking the derivative of the error:

$$\dot{e}_{r1} = \dot{\phi}_d - \dot{\phi} = \dot{\phi}_d - p \tag{7}$$

Set the Lyapunov function :

$$V(e_{r1}) = \frac{1}{2} e_{r1}^2 \tag{8}$$

Taking the derivative of the Lyapunov function :

$$\dot{V}(e_{r1}) = e_{r1} \dot{e}_{r1} \tag{9}$$

Define virtual control term a_{rd} and set

$$e_{r2} = p - a_d \tag{10}$$

In order to make $e_{r1} \to 0$, $p \to \dot{\phi}_d$ .Set $a_d = -c_{r1} e_{r1} + \dot{\phi}_d$.

$$\begin{aligned} \dot{V}(e_{r1}) &= e_{r1}(e_{r2} + a_d - \dot{\phi}_d) \\ &= e_{r1}(e_{r2} - c_{r1} e_{r1} + \dot{\phi}_d - \dot{\phi}_d) \\ &= e_{r1}(e_{r2} - c_{r1} e_{r1}) \\ &= -c_{r1} e_{r1}^2 + e_{r1} e_{r2} \end{aligned} \tag{11}$$

To avoid differential explosions caused by $\dot{a}_d$, This disadvantage can be overcome by using a low-pass filter. Output of low-pass filter with a_d as $\overline{p}$, τ_d is the time constant of the first-order filter, defined $\overline{p} = -c_{r1} e_{r1} + \dot{\phi}_d$ and satisfied

$$\begin{cases} \tau_d \dot{a}_d + a_d = \overline{p} \\ a_d(0) = \overline{p}(0) \end{cases} \tag{12}$$

Can get $\dot{a}_d = \tau_d^{-1} \overline{p} - \tau_d^{-1} a_d$, the filtering error is $y_{r2} = a_d - \overline{p}$.

Considering position tracking, virtual control variables, and filter errors, set the Lyapunov function

$$V_2 = \frac{1}{2} e_{r1}^2 + \frac{1}{2} e_{r2}^2 + \frac{1}{2} y_{r2}^2 \tag{13}$$

Due to

$$\begin{aligned} &= f(\omega) + g(\omega) l_d - \dot{a}_d \\ \dot{y}_{r2} &= \tau_d^{-1} \overline{p} - \tau_d^{-1} a_d - \dot{\overline{p}} \\ &= -\tau_d^{-1} y_{r2} + c_{r1} \dot{e}_{r1} - \ddot{\phi}_d \end{aligned} \tag{14}$$

can be inferred

$$\begin{aligned} \dot{V}_2 &= e_{r1}(e_{r2} + y_{r2} + \overline{p} - \dot{\phi}_d) \\ &+ e_{r2}(f(\omega) + g(\omega) l_d - \dot{a}_d) \\ &+ y_{r2}(-\tau_d^{-1} y_{r2} + c_{r1} \dot{e}_{r1} - \ddot{\phi}_d) \\ &= e_{r1}(e_{r2} + y_{r2} + \overline{p} - \dot{\phi}_d) \\ &+ e_{r2}(f(\omega) + g(\omega) l_d - \dot{a}_d) \\ &+ y_{r2}(-\tau_d^{-1} y_{r2} + B_{r2}) \\ B_{r2} &= c_{r1} \dot{e}_{r1} - \ddot{\phi}_d \end{aligned} \tag{15}$$

B_{r2} is the function of e_{r1} , e_{r2} , y_{r2}

$$\begin{aligned} B_{r2} &= c_{r1}(p - \dot{\phi}_d) - \ddot{\phi}_d \\ &= c_{r1}(e_{r2} + a_d - \dot{\phi}_d) - \ddot{\phi}_d \\ &= c_{r1}(e_{r2} + y_{r2} + \overline{p} - \dot{\phi}_d) - \ddot{\phi}_d \\ &= c_{r1}(e_{r2} + y_{r2} - c_{r1} e_{r1}) - \ddot{\phi}_d \end{aligned} \tag{16}$$

Design the controller as:

$$l_d = (g(\omega))^{-1}(-f(\omega) + \dot{a}_d - c_{r2} e_{r2}) \tag{17}$$

B. Proof of adaptive filtering backstepping control law

Taking the roll system as an example, the proof of the control law is as follows.

When $V_2(0) \le \vartheta$, $\vartheta > 0$, then all signals in the closed-loop system converge with bounds.

Prove: when $V_2 = \vartheta$, $V_2 = \frac{1}{2} e_{r1}^2 + \frac{1}{2} e_{r2}^2 + \frac{1}{2} y_{r2}^2 = \vartheta$, B_{r2} bounded, set M_{r2} ,can get $\frac{B_{r2}^2}{M_{r2}^2} - 1 \le 0$.

$$\begin{aligned} \dot{V}_2 &= e_{r1}(e_{r2} + y_{r2}) \\ &- c_{r1} e_{r1}^2 - c_{r2} e_{r2}^2 + y_{r2}(-\tau_d^{-1} y_{r2} + B_{r2}) \\ &\le \frac{1}{2}(e_{r1}^2 + e_{r2}^2) + \frac{1}{2}(e_{r1}^2 + y_{r2}^2) \\ &- c_{r1} e_{r1}^2 - c_{r2} e_{r2}^2 - \tau_d^{-1} y_{r2}^2 + \frac{1}{2} y_{r2}^2 B_{r2}^2 + \frac{1}{2} \\ &= (1 - c_{r1}) e_{r1}^2 + (\frac{1}{2} - c_{r2}) e_{r2}^2 \\ &+ (\frac{1}{2} B_{r2}^2 + \frac{1}{2} - \tau_d^{-1}) y_{r2}^2 + \frac{1}{2} \end{aligned} \tag{18}$$

Take positively definite κ, $\varepsilon_{p} = 1 + \kappa$, $\varepsilon_{r} = \frac{1}{2}\beta + \kappa$, $G_{i}^{2} \ge \frac{1}{2} M_{i3} + \frac{1}{2} + \kappa$

$$
\begin{aligned}
\dot{V}_{2} &\le -\kappa e_{\omega}^{2} - \kappa e_{\omega 3}^{2} + (\frac{1}{2} R_{i}^{2} - \frac{1}{2} M_{i}^{2} - \kappa) e_{\omega}^{2} + \frac{1}{2} \\
&= -2\kappa V_{1} + (\frac{M_{i3}^{2}}{2 M_{i3}^{2}} R_{i}^{2} - \frac{1}{2} M_{i}^{2}) e_{\omega 3}^{2} + \frac{1}{2} \le 0 \\
&= -2\kappa V_{1} + (\frac{R_{i}^{2}}{M_{i3}^{2}} - 1) \frac{M_{i3}^{2} e_{\omega}^{2}}{2} + \frac{1}{2} \le 0
\end{aligned}
\qquad (19)
$$

Take $\kappa \ge \frac{1}{4\beta}$, can get $\dot{V}_{1} \le -2\frac{1}{4\beta}\beta + \frac{1}{2} = 0$

Therefore, it can be proven that when $V_{1}(0) \le \beta$, $V_{2}(t) \le \beta$, the system converges. Similarly to the roll system, the control laws of the attitude control system in three directions can be obtained as follows. M_{l1}, M_{m1}, M_{n1} are three-axis adaptive items.

$$
\begin{cases}
l_{d} = (u_{d} - c_{l3} e_{l3}) M_{l3} + (J_{yy} - J_{zz}) qr - M_{l1} \\
m_{d} = (u_{m} - c_{m3} e_{m3}) M_{l3} + (J_{zz} - J_{xx}) pr - M_{m1} \\
n_{d} = (u_{n} - c_{n3} e_{n3}) M_{l3} + (J_{xx} - J_{yy}) pq - M_{n1}
\end{cases}
\qquad (20)
$$

In a normal state, the expected roll torque is fully borne by a pair of ailerons, the expected pitch torque is fully borne by a pair of elevators, and the expected yaw torque is fully borne by the rudder. The expected deviation angle of the control surface is interpolated based on the expected torque table.

C. Error tolerance allocation for quadratic programming control surface

The basic principle of command allocation on the control surface is to ensure that the control torque generated by the control surface is consistent with the expected value when the control surface is damaged. The aerodynamic torque of UAV is a nonlinear function, and the aerodynamic derivatives in Θ_{1} and Θ_{2} are time-varying parameters. Based on the control surface sensor, the specific defect or floating situation of the control surface can be quickly and accurately obtained, and the steering effect Θ_{2} of each control surface can be corrected by multiplying the defect parameters according to the damage situation. u_{2d} is the input of the control surface without damage. From the expected three-axis torque, it can be inferred that the control torque generated by the expected control surface is

$$
M_{E} = \Theta_{2} u_{2d} = M - \Theta_{1}\Phi_{1} \qquad (21)
$$

After damage occurs to the control surface, paired control of the ailerons, flaps, elevators, and rudder will no longer be carried out according to normal flight. All control surfaces are reconstructed and operated independently. At this point, the control matrix Θ_{2} will become Θ_{2b}.

In order to maximize the strengths of each control surface, set $\|W_{u}(u_{2} - u_{2d})\|_{2}^{2}$ to make the steering effect as close as possible to the expected value of the control law, set $\|W_{e}(\Theta_{2b} u_{2} - M_{E})\|_{2}^{2}$ to reduce control surface jitter, set $\|W_{du}(u_{2} - u_{2d-1})\|_{2}^{2}$ to reduce vertical surface saturation, set $\|W_{s} u_{2}\|_{2}^{2}$, and establish a quadratic programming model as follows

$$
\left.
\begin{aligned}
& J = \gamma_{1}\|W_{u}(u_{2} - u_{2d})\|_{2}^{2} \\
\min \quad & + \gamma_{2}\|W_{e}(\Theta_{2b} u_{2} - M_{E})\|_{2}^{2} \\
& + \gamma_{3}\|W_{du}(u_{2} - u_{2d-1})\|_{2}^{2} + \gamma_{4}\|W_{s} u_{2}\|_{2}^{2} \\
\text{s.t.} \quad & \delta_{ae}(t) \in [-30^{\circ}, 30^{\circ}], \ \delta_{r}(t) \in [0^{\circ}, 30^{\circ}]
\end{aligned}
\right\}
\qquad (22)
$$

M_{E} is the expected torque, W_{u}, W_{e}, W_{du}, W_{s} are the weight matrices, u_{2d-1} is the input of the control surface of the previous control step, and γ_{1}, γ_{2}, γ_{3}, γ_{4} are positive weight coefficients.

Deformation of equation (22)

$$
\begin{aligned}
J &= \gamma_{1}(u_{2} - u_{2d})^{T} W_{u}(u_{2} - u_{2d}) \\
&+ \gamma_{2}(\Theta_{2b} u_{2} - M_{E})^{T} W_{e}(\Theta_{2b} u_{2} - M_{E}) + \\
&\gamma_{3}(u_{2} - u_{2d-1})^{T} W_{du}(u_{2} - u_{2d-1}) + \gamma_{4} u_{2}^{T} W_{s} u_{2} \\
&= \gamma_{1}(u_{2}^{T} W_{u} u_{2} - u_{2}^{T} W_{u} u_{2d} - u_{2d}^{T} W_{u} u_{2} + u_{2d}^{T} W_{u} u_{2d}) \\
&+ \gamma_{2}(u_{2}^{T} \Theta_{2b}^{T} W_{e} \Theta_{2b} u_{2} - u_{2}^{T} \Theta_{2b}^{T} W_{e} M_{E} \\
&- M_{E}^{T} W_{e} \Theta_{2b} u_{2} + M_{E}^{T} W_{e} M_{E}) + \\
&\gamma_{3}(u_{2}^{T} W_{du} u_{2} - u_{2}^{T} W_{du} u_{2d-1} - u_{2d-1}^{T} W_{du} u_{2} + u_{2d-1}^{T} W_{du} u_{2d-1}) \\
&+ \gamma_{4} u_{2}^{T} W_{s} u_{2} \\
&= u_{2}^{T}(\gamma_{1} W_{u} + \gamma_{2} \Theta_{2b}^{T} W_{e} \Theta_{2b} + \gamma_{3} W_{du} + \gamma_{4} W_{s}) u_{2} \\
&+ u_{2}^{T}(-2\gamma_{1} W_{u} u_{2d} - 2\gamma_{2} \Theta_{2b}^{T} W_{e} M_{E} - 2\gamma_{3} W_{du} u_{2d-1}) + \\
&(\gamma_{1} u_{2d}^{T} W_{u} u_{2d} + \gamma_{2} M_{E}^{T} W_{e} M_{E} + \gamma_{3} u_{2d-1}^{T} W_{du} u_{2d-1}) \\
&= \frac{1}{2} u_{2}^{T} T u_{2} + u_{2}^{T} D + R
\end{aligned}
\qquad (23)
$$

For simulation programs that run on periodic sampling, removing constants R does not affect finding the optimal solution. Equation (23) can be transformed into a standard quadratic programming form.

$$
\left.
\begin{aligned}
\min \quad & J = \frac{1}{2} u_{2}^{T} T u_{2} + u_{2}^{T} D \\
\text{s.t.} \quad & \delta_{ae}(t) \in [-30^{\circ}, 30^{\circ}], \ \delta_{r}(t) \in [0^{\circ}, 30^{\circ}]
\end{aligned}
\right\}
\qquad (24)
$$

In the equation, $T = 2\gamma_{1} W_{u} + 2\gamma_{2} \Theta_{2b}^{T} W_{e} \Theta_{2b} + 2\gamma_{3} W_{du} + 2\gamma_{4} W_{s}$ and $D = -2\gamma_{1} W_{u} u_{2d} - 2\gamma_{2} \Theta_{2b}^{T} W_{e} M_{E} - 2\gamma_{3} W_{du} u_{2d-1}$. The calculated vector u_{2} is the allocation result of the deviation angles of each control surface.

D. RBF Neural network fitting adaptive term

RBF neural network, as a typical nonlinear function approximator, can fit any nonlinear function, and has extensive engineering applications in the field of aircraft control. This article introduces RBF neural network to fit the uncertain adaptive terms of the system model, ensuring the performance of the closed-loop control system.

In RBF networks, $X=[X_1 \quad X_2 \quad \dots \quad X_n]^T$ is the input vector of the network. Let the radial basis vector of the RBF neural network be $H=[h_1 \quad h_2 \quad \dots \quad h_q]^T$, where h_j is the Gaussian basis function

$$h_j=\exp\left(-\frac{\|X-C_j\|^2}{2b_j^2}\right) \quad (j=1,2\cdots q) \tag{25}$$

The center vector of the j-th node of the network is $C_j=[C_{j1} \quad C_{j2} \quad \dots \quad C_{jn}]^T$

Set the base width vector of the network to $B=[b_1 \quad b_2 \quad \dots \quad b_q]^T$, where b_j is the base width parameter of node i and is a number greater than zero. The weight vector of the network is $W=[w_1 \quad w_2 \quad \dots \quad w_q]^T$

The output of the identification network is

$$M_a(k)=w_1h_1+w_2h_2+\cdots+w_qh_q \tag{26}$$

The performance indicator function is as follows: $\sigma_d(k)$ is the expected attitude angle of the k-th step, and $\sigma(k)$ is the actual attitude angle of the k-th step

$$J=\frac{1}{2}(\sigma_d(k)-\sigma(k))^2 \tag{27}$$

The sensitivity of the output of the Jacobian term $\frac{\partial\sigma(k)}{\partial M_a}$ to change in control input is identified through RBF neural networks, and the iterative algorithm is as follows:

$$\frac{\partial\sigma(k)}{\partial M_a}\approx\frac{\partial\sigma_a(k)}{\partial M_a}=\sum_{j=1}^{q}w_jh_j\frac{c_{ji}-M_a(k)}{b_j^2} \tag{28}$$

According to the gradient descent method, the iterative algorithm for output weight, node center, and node base width parameters is as follows, where η is the learning rate, and λ_1, λ_2 are the inertia coefficients.

$$\begin{aligned}
&\Delta w_j=(\sigma_d(k)-\sigma(k))h_j\frac{\partial\sigma(k)}{\partial M}\\
&w_j(k)=w_j(k-1)+\eta\Delta w_j\\
&+\lambda_1(w_j(k-1)-w_j(k-2))+\lambda_2(w_j(k-2)-w_j(k-3))\\
&\Delta b_j=(\sigma_d(k)-\sigma(k))w_jh_j\frac{\|X-C_j\|^2}{b_j^3}\\
&b_j(k)=b_j(k-1)+\eta\Delta b_j\\
&+\lambda_1(b_j(k-1)-b_j(k-2))+\lambda_2(b_j(k-2)-b_j(k-3))\\
&\Delta c_{ji}=(\sigma_d(k)-\sigma(k))w_jh_j\frac{X_j-c_{ji}}{b_j^2}\\
&c_{ji}(k)=c_{ji}(k-1)+\eta\Delta c_{ji}\\
&+\lambda_1(c_{ji}(k-1)-c_{ji}(k-2))+\lambda_2(c_{ji}(k-2)-c_{ji}(k-3))
\end{aligned} \tag{29}$$

Set the number of input nodes in three directions to 3, so that the adaptive identification inputs are $X_{\phi}=[\phi \quad \phi_d-\phi \quad p]^T$, $X_{\theta}=[\theta \quad \theta_d-\theta \quad q]^T$; and $X_{\psi}=[\psi \quad \psi_d-\psi \quad r]^T$, respectively. Set the number of intermediate layer nodes to 6, the number of output nodes to 1, the initial center vector to 0 vector, and the initial base width vector to 0 vector. In simulation operation, the weight coefficients can be quickly converged to compensate for the control amount of the filtering backstepping method. The flowchart of adaptive item calculation is shown in figure 2.

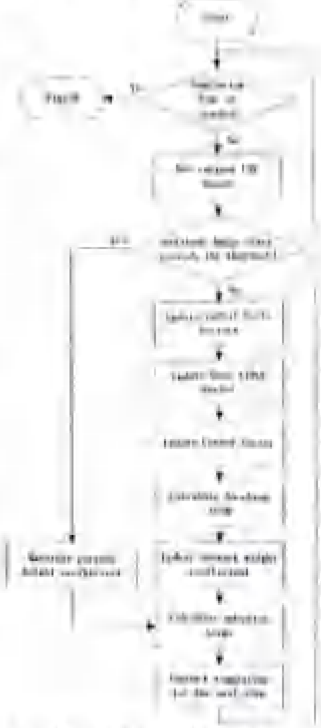

Figure 2 Adaptive item calculation flowchart

The relationship between neural networks and control laws and allocation laws is shown in the figure 3.

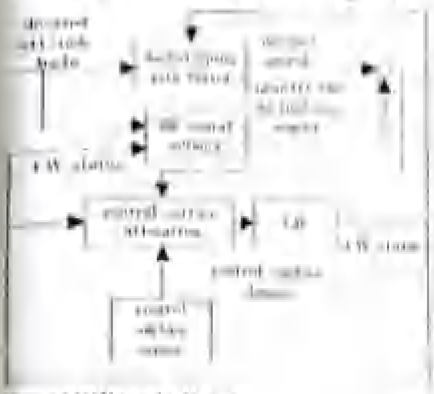

Figure 3 UAV control architecture

IV. SIMULATION VERIFICATION

(1)UAV parameter in table I

TABLE I UAV PARAMETER

Parameter	Value
mass	150.3kg
inertia (J_x, J_y, J_z)	(13.59, 159.22, 169.46) kg m2
Wingspan b	3.72 m
MAC c	0.349 m
Main wing reference area S	1.39m2
Servo damping ratio ξ	0.7
Servo natural frequency ω_n	62.8

(2)Controller parameter in TABLE II

TABLE II CONTROLLER PARAMETER

Parameter	Value
c_{rl1}	15.41
c_{rl2}	3.96
c_{pi1}	9.88
c_{pi2}	5.76
c_{ya1}	5.14
c_{ya2}	6.32
r_{rl}	1
r_{pi}	1
r_{ya}	1

(3)Allocator parameter in TABLE III

TABLE III ALLOCATOR PARAMETER

Parameter	Value
γ_1	1
γ_2	1
γ_3	100
γ_4	1

Tip: W_u, W_v, W_w, W_l is the identity matrix.

(4)Neural network parameter in table IV

TABLE IV NEURAL NETWORK PARAMETER

Parameter	Value
$\eta_{r1}, \eta_{p1}, \eta_{y1}$	0.4
$\lambda_{r1}, \lambda_{p1}, \lambda_{y1}$	0.05
$\lambda_{r2}, \lambda_{p2}, \lambda_{y2}$	0.01

Taking the following different control surface damage situations in TABLE V as examples, UAVs can quickly return to a stable flight state and respond to the commanded attitude angle. The result is shown in figures 4-6.

TABLE V CONTROL SURFACE PARAMETER

	Case 1	Case 2	Case 3	Case 4	Case 5	Case 6	Case 7	Case 8
LA	100%	50%	0%	100%	0%	50%	100%	50%
RA	100%	100%	0%	100%	0%	50%	100%	50%
LF	100%	100%	100%	100%	100%	100%	100%	10%
RF	100%	100%	100%	100%	100%	100%	100%	0%
LE	100%	100%	100%	50%	50%	100%	100%	100%
RE	100%	100%	100%	50%	50%	100%	0%	100%
R	100%	100%	100%	100%	100%	0%	100%	100%

Tip: LA is left aileron remaining, RA is right aileron remaining, LF is left flap remaining, RF is right flap remaining, LE is left elevator remaining, RE is right elevator remaining, R is rudder remaining

The UAV adopts BTT turning mode, and the UAV changes the roll Angle when the track route needs to be changed. The side force generated by the roll drives the body to generate the corresponding heading Angle. The roll Angle and yaw Angle change the track at the same time to achieve the effect of changing the track and route, so no instructions are applied to the yaw direction.

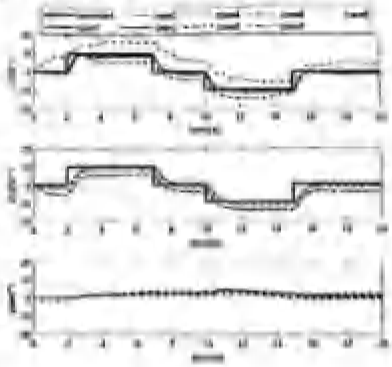

Figure 4 UAV response to commands

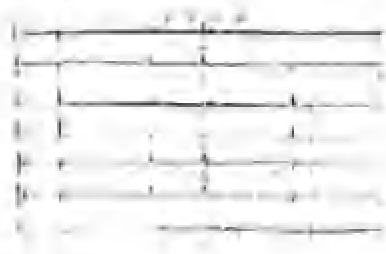

Figure 5 Control surface actuation of UAV

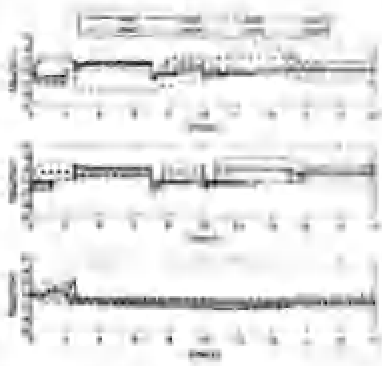

Figure 6 Changes of adaptive terms

V. Conclusion

This paper takes multi-control surface UAV as the research object, and conducts research on the issues of control surface defects and floating. The following conclusions are drawn:

(1) The adaptive filtering backstepping algorithm effectively solves the expected control torque of multi-control surface UAVs. The controller which equipped with a filter can solve the problem of differential explosion by adjusting the filter time constant parameter, which has high engineering application value. The RBF fitting adaptive term can provide output compensation when the attitude angle error of the UAV is large, and improve control accuracy when the attitude angle error is small.

(2) The quadratic programming allocation algorithm adjusts the steering effectiveness matrix in real-time based on the defect and floating situation transmitted by the control surface sensors, and models the control surface to achieve fast and accurate results. The control effectiveness, saturation and jitter vibration of control surfaces are taken into consideration to avoid attitude divergence during high-speed flight of UAV.

(3) Simulations under various typical control surface damage scenarios have shown that establishing dynamic and kinematic models based on the dynamic characteristics of UAVs, designing attitude control algorithms, control surface allocation algorithms, and adaptive term identification algorithms can enable UAVs to continue tracking the target attitude angle and continue flight on the route. This control algorithm can effectively improve the survival rate of UAVs.

Acknowledgment

1) Jiangsu Province introduces the "Thousand Talents Plan" to cultivate high-level talents for innovation and entrepreneurship, project number: [illegible]

2) Jiangsu Province's major scientific and technological research and development project "Universal Emergency Rescue Intelligent Air Robot System", project number: [illegible]

References

[1] CHEN [illegible] et al. [illegible] Flight Control of UAV: A Survey[J]. [illegible]

[2] MA J, LI W, LI P, et al. Research Status and Prospects of Aircraft Control Allocation Technology[J]. Flight Dynamics, 2009, 27(03): [illegible]

[3] WANG [illegible], GAO [illegible], LI W. [illegible] Multi-object Nonlinear Control Allocation Method[J]. Flight Dynamics, 2008 [illegible]

[4] Zhang X, Ma X, Chen [illegible], et al. Hybrid multi-objective control allocation strategy for reusable launch vehicle in re-entry phase[J]. Aerospace Science and Technology, [illegible]

[5] ZHAO X. Aerodynamic Surrogate Model Design and Control Allocation of Flying Wing Unmanned Aerial Vehicle for High Efficiency[D]. University of Chinese Academy of Sciences[illegible] [illegible]

[6] CUI Y, ZHANG W, LI C, et al. Research on Reconstruction Control of Multiple Control Surfaces Based on Linear Programming[J]. Flight Dynamics, 201[illegible]

[7] Bodson M. Evaluation of optimization methods for control allocation[J]. Journal of Guidance, Control, and Dynamics, 2002, 25(4): 703-711.

[8] Härkegård O. Backstepping and control allocation with applications to flight control[D]. Linköpings universitet, 2003.

[9] Liu X, Du Z, Yang Z, et al. Real-Time Control Allocation for Autonomous Surface Vehicle Using Constrained Quadratic Programming[J]. [illegible] Navigation and Control(English), [illegible]

[10] CHEN Y, DONG X, XUE J, et al. Robust linear parameter-varying predictive tracking control scheme for over-actuated surface[J]. Control Theory & Applications, 2013 [illegible]

[11] LV Y, ZHANG W, SHI J, et al. A Practical Nonlinear Control Allocation Method Based on Rudder Position Feedback[J]. Journal of Beijing University of Aeronautics and Astronautics, 2016, 42(0[illegible])

[12] Shtessel Y, McDuffie J, Jackson M, et al. Sliding mode control of the X-33 vehicle in launch and re-entry modes[C]. Guidance, Navigation and Control Conference and Exhibit, 1998: 4414.

[13] XV J, [illegible]. Research on Flight Control Technology of Folding Control Reconfigurable [illegible] UAV[J]. Ordnance Industry Automation, 2022, 41(0[illegible]): 92-96.

[14] [illegible] A, Richard B, Dominik M. An Approximate Backstepping Based Trajectory Tracking Control of a Gun Launched Micro Aerial Vehicle in Crosswind[J]. Journal of Intelligent & Robotic Systems, 2013, 70(1-4): [illegible]

[15] LI H, ZHANG Y, SHI L, et al. Global set-stable nonlinear adaptive dynamic control allocation for aircraft with multiple control effectors[J]. Control and Decision, 2013, 28(0[illegible])

[16] MA Y, SHI X, LIU H, et al. Adaptive Neural Network Fault Tolerant Control of [illegible] Vehicle Attitude System[J]. Journal of Astronautics, 2021, 42(0[illegible])

[17] Cai X, Qiu H, Gao L, et al. Adaptive radial-basis-function-based multifidelity metamodeling for expensive black-box problems[J]. AIAA journal, 2017, 55(7): 2424-2436.